FGFR1 is critical for *Rbl2* loss-driven tumor development and requires PLCG1 activation for continued growth of small cell lung cancer

Authors and Affiliations:

Kee-Beom Kim[1], Youngchul Kim[2], Dong-Wook Kim[1, 3, 4], Kwon-Sik Park[1, 4, 5]

[1] Department of Microbiology, Immunology, and Cancer Biology, University of Virginia, Charlottesville, VA 22908, USA

[2] Department of Biostatistics and Bioinformatics, Moffitt Cancer Research Center Tampa Bay, FL 33612, USA

[3] Bionanotechnology Research Center, Korea Research Institute of Bioscience and Biotechnology, Daejeon, 34141, Republic of Korea

[4] Co-corresponding authors

[5] Lead contact: Kwon-Sik Park, 1340 Jefferson Park Avenue, Charlottesville, VA 22908, USA; E-mail: kp5an@virginia.edu; Phone: 434-982-1947

Running Title: Oncogenic role of FGFR1 in SCLC

Abstract

Small cell lung cancer (SCLC) remains a recalcitrant disease; limited therapeutic options have not improved overall survival and approved targeted therapies are lacking. Amplification of the tyrosine kinase receptor FGFR1 (fibroblast growth factor receptor 1) is one of the few actionable alterations found in SCLC genome. However, efforts to develop targeted therapies for *FGFR1*-amplified SCLC are hindered by critical gaps in knowledge around the molecular origins and mediator of FGFR1-driven signalling and the physiological impact of targeting FGFR1. Here we demonstrate the oncogenic impact of increased FGFR1 on the malignant progression of precancerous cells and the necessity of nonamplified *FGFR1* for SCLC development and homeostasis. Unexpected dependency of *Rbl2* loss-driven tumor development on FGFR1 in autochthonous mouse models reveals a novel function of p130 (encoded by *Rbl2*), a member of the RB family of tumor suppressors, as a regulator of FGFR1 expression. Additionally, FGFR1-dependent SCLC cells require activation of PLCG1 for continued growth. Together, this study uncovers mechanisms of FGFR1-driven SCLC that involves p130 upstream and PLCG1 downstream and provides potential biomarkers for anti-FGFR1 therapeutic strategy.

Key Words: SCLC, FGFR1, RBL2, PLCG1, mouse model

Introduction

SCLC accounts for approximately 13% of all lung cancer and remains a recalcitrant disease. The standard chemotherapy of cisplatin and etoposide has not significantly improved overall survival in SCLC patients and the development of targeted therapies has been challenging due to the paucity of clinically viable targets (1). SCLC is mostly driven by loss of tumor suppressors, including near universal inactivation of RB and p53 and frequent loss of other tumor suppressors such as the RB family members p107 and p130 (coded by the *RBL1* and *RBL2*, respectively) (2, 3). Unfortunately, these loss-of-function alterations are not directly actionable. Although oncogenic alterations are less frequent in SCLC, gene amplifications of *FGFR1* are detected in approximately 6% of SCLC tumors and high FGFR1 expression is also detected in a subset of tumors without the gene amplification (2-6). Importantly, an FGFR-selective tyrosine kinase inhibitor (TKI) can inhibit the growth of SCLC cell lines with high FGFR1 expression (7-9). However, *FGFR1* amplification and high FGFR1 levels alone do not guarantee sensitivity to FGFR inhibitors (7-9). Intracellular mediators of FGFR1 signaling as well as other genetic alterations may modulate sensitivity to treatment, but these mechanisms remain poorly defined. For example, while the MEK-ERK pathway mediates oncogenic FGFR1 signaling in some SCLC cell lines, a hyperactive RAF-MEK-ERK pathway is tumor suppressive in others (10, 11). In addition, while AKT, STAT, and PLCG1 act as transducers downstream of FGFR1 during organ development, little is known of their roles in SCLC (12). Importantly, physiological

65 significance of FGFR1, either amplified or nonamplified, in SCLC has not formally
66 been determined using autochthonous model. The oncogenic role has also
67 recently been challenged by a study in which a constitutively active form of FGFR1
68 suppressed SCLC development in *Rb1/Trp53*-mutant genetically engineered
69 mouse model (*Rb1/Trp53*-GEMM) (13). Thus, there are critical gaps in knowledge
70 that need to be addressed not only to target FGFR1 in SCLC, but also to identify
71 SCLC patients in ongoing clinical trials who would benefit from anti-FGFR1
72 therapies.
73
74 Here, we characterize FGFR1 in SCLC using *Rb1/Trp53*-GEMM and its variants
75 in which adenoviral Cre (Ad-Cre)-mediated deletion of *Rb1* and *Trp53* results in
76 lung tumors recapitulating major histopathological features of human SCLC
77 (14,15). We also introduced genetic and chemical perturbations in primary tumor
78 cells (mSCLC) as well as precancerous neuroendocrine cells (preSC) derived from
79 the *Rb1/Trp53*-GEMM and that can transform into SCLC upon activation of
80 oncogenic drivers (16). Our data show that FGFR1 is required for the development
81 and growth of *Rbl2* loss-driven SCLC, and that this dependency is due to the
82 induction of FGFR1 expression. Furthermore, FGFR1 promotes tumor
83 development and growth via activation of PLCG1 and alteration in neural
84 differentiation. Taken together, our findings provide insight into the mechanism of
85 SCLC progression and potential biomarkers for identifying patients appropriate for
86 anti-FGFR1 therapies.

87 **Materials and Methods**

88

89 *Plasmids and chemicals*

90 All plasmids used in this study are listed in Supplementary Table 1. The sequences
91 of shRNAs and gRNAs are listed in Supplementary Table 2 and 3. *Fgfr1* cDNA
92 was cloned using total RNAs from murine SCLC cells and verified by Sanger
93 sequencing. U73122 and U73343 were obtained from Cayman and PD173074
94 from Sigma.

95

96 *Cell culture*

97 Murine SCLC cells (mSCLC) and precancerous cells (preSC) were derived from
98 lung tumors and early-stage neuroendocrine lesions, respectively, developed in
99 the *Rb1/Trp53*-GEMM (16). Human SCLC cell lines (NCI-H82, NCI-H209, NCI-
100 H524, also designated simply as H82, H209, H524) were obtained from ATCC.
101 293T cells were cultured in DMEM media and human and mouse cells were
102 cultured in RPMI1640 media, both supplemented with 10% bovine growth serum
103 (GE Healthcare) and 1% penicillin-streptomycin (Invitrogen). Puromycin (Thermo
104 Fisher) was used to select stably transduced cells following lentiviral infection. For
105 lentivirus production we transfected lentiviral plasmids with packaging plasmids in
106 293T cells using polyethylenimine (Sigma), harvested supernatants containing
107 viral particles 48 and 72 hours later, filtered through 0.45μm PVDF filter before
108 adding to culture of target cells in the presence of 5μg/ml polybrene (Sigma). To
109 induce FGFR1 expression in *Fgfr1-preSC*, cells were treated with doxycycline

110 (0.2ug/mL). CRISPR-mediated knockout of *Rbl2* was achieved by transient
111 transfection of Cas9 and gRNA in a single vector using Lipofectamine 2000
112 (Invitrogen). Forty-eight hours later, transfected cells were enriched by FACS
113 sorting for red fluorescent protein expressed from the same vector. Sanger
114 sequencing verified mutation in the target sequence in *Rbl2* gene and immunoblot
115 validated loss of p130 coded by *Rbl2*. MTT assay was performed to measure cell
116 viability using thiazolyl blue tetrazolium bromide (Sigma). Cells were seeded at 1
117 $\times 10^4$ per well in 96-well plates at day 0, and MTT reagents were added on day 4.
118 O.D values were determined at a wavelength of 590 nm using an ELISA reader
119 (Thermo Scientific) The percentage survival was determined as the ratio of treated
120 cells versus vehicle control after background subtraction. Soft-agar assay was
121 performed by seeding $1x10^4$ cells per well in 12-well plates as previously described
122 (16). Images of wells are acquired using Olympus MVX10 scope, and colonies
123 from the whole field of image were counted using the imaging software NIS-
124 Elements Basic Research (Nikon). All of the cell culture experiments were
125 performed in triplicates and repeated for a minimum of two biological replicates.
126

127 *Tumor induction and allograft*

128 *Rb1*$^{lox/lox}$*; Trp53*$^{lox/lox}$ (*Rb1/Trp53*-GEMM) and *Rb1*$^{lox/lox}$*; Trp53*$^{lox/lox}$*; Rbl2*$^{lox/lox}$
129 (*Rb1/Trp53/Rbl2*-GEMM) have been previously described (14, 16). Mouse strains
130 with *Fgfr1*^{lox} and *Fgfr2*^{lox} alleles have been previously described (17, 18). For tumor
131 induction, lungs of 10-week-old mice were infected with adenoviral Cre via
132 intratracheal instillation as previously described and mice were aged 6 months

133 (19). For allograft experiment, we inject 5.0×10^5 control or *Fgfr1*-preSC in the flanks
134 of nude mice (*Foxn1*$^{nu/nu}$; Envigo) and 1.0×10^6 *Fgfr1*$^{lox/lox}$ *Rb1/Trp53/Rbl2* murine
135 cells infected with Ad-Cre in the flanks of B6/129S F1 hybrid mice (Jackson
136 Laboratory). To induce FGFR1 expression in *Fgfr1*-preSC following implantation,
137 mice were fed doxycycline diet (625mg/kg, Envigo). Mice were maintained
138 according to guidelines from the National Institutes of Health. Animal procedures
139 were approved by the Animal Care and Use Committee at the University of
140 Virginia.
141
142 *Histology, immunohistochemistry, and immunoblot*
143 Mouse tissues were fixed in 4% paraformaldehyde in phosphate-buffered saline
144 before paraffin embedding. Five micrometer-thick tissue sections were stained
145 with hematoxylin and eosin staining and immunostaining as previously described
146 (16). For quantification of pHH3-positive cells, tumors of similar size and area were
147 included. For immunoblot analysis, protein was extracted from mouse tumor
148 tissues and human and murine cell lines in RIPA buffer. All primary and secondary
149 antibodies used are listed in Supplementary Table 4. Macroscopic images of lung
150 sections were acquired using Olympus MVX10. Images of H&E and
151 immunostained tissues were acquired using Nikon Eclipse Ni-U microscope.
152 Image analysis and automated quantification were performed using NIS-Elements
153 Basic Research (Nikon)
154
155 *RNA sequencing and analysis*

156 Sequencing libraries were generated by the Genome Analysis and Technology
157 Core at University of Virginia using oligo dT-purified mRNA from 500ng of total
158 RNA and the NEB Next Ultra RNA library preparation kit (New England Biolabs),
159 and 50-bp single-end sequencing was performed on Illumina NextSeq 500
160 platform (Illumina). The sequencing data have been deposited to the SRA
161 Database (https://www.ncbi.nlm.nih.gov/sra, identifier: PRJNA564798). Reads
162 were mapped to the Mus musculus genome assembly GRCm38 (mm10) using
163 TopHat and counts of reads map to each gene were obtained using HTSeq (20,
164 21). Differentially expressed genes regulated by FGFR1 were identified using
165 DESeq2 package (22). A regularized log-transformation was applied to the read
166 count data of all sequenced samples and resultant data were used for gene
167 ontology (GO) term analysis at DAVID Bioinformatics Resources
168 (https://david.ncifcrf.gov/home.jsp).
169
170 *Statistical analysis*
171 Using GraphPad Prism, the results were presented as the mean ± standard
172 deviation. and evaluated using an unpaired two-tailed Student's t-test. $p<0.05$ was
173 considered statistically significant.
174

175 **Results**

176

177 ***Ectopic FGFR1 promotes progression of precancerous cells to SCLC***

178 The lung tumors in *Rb1/Trp53*-GEMM, unlike a subset of human SCLC tumors,
179 have not shown *Fgfr1* amplification (3, 23). Instead, cell derivatives of these lung
180 tumors (murine SCLC, mSCLC) showed markedly higher levels of *Fgfr1* mRNA
181 and FGFR1 protein than precancerous cells (preSC) (Fig. 1A). To begin
182 determining the functional impact of these alterations on tumor development, we
183 expressed FGFR1 in preSC using a lentiviral vector and tested the transduced
184 cells for tumorigenic potential. Compared with control preSC infected with empty
185 vector, *Fgfr1*-preSC gave rise to more colonies in soft agar and more rapid
186 development of subcutaneous tumors in immunocompromised nude mice (Fig. 1B,
187 C). These subcutaneous tumors displayed histological features of SCLC including
188 distinct small-cell morphology with scanty cytoplasm and positive staining for the
189 neuroendocrine marker calcitonin gene-related peptide (CGRP) (Fig. 1D). These
190 data suggest that FGFR1 overexpression is sufficient to promote tumorigenic
191 transformation of precancerous precursors.

192

193 ***Deletion of FGFR1 suppresses Rbl2-deficient SCLC***

194 The physiological significance of FGFR1 in SCLC has not been formally validated
195 in autochthonous model. To begin testing whether FGFR1 is required for SCLC
196 development *in vivo*, we deleted *Fgfr1* in *Rb1/Trp53*-GEMM carrying *Fgfr1*$^{lox/lox}$
197 alleles using intratracheal instillation of Ad-Cre. We found that there was no

198 significant difference in tumor burden (tumor area/lung area) between *Fgfr1*$^{\Delta/\Delta}$ and
199 *Fgfr1*$^{+/+}$ *Rb1*/*Trp53* controls (Fig. 2A). This indicates that in *Rb1*/*Trp53*-mutant
200 mSCLC, FGFR1 is likely dispensable for tumor development even though its
201 overexpression was sufficient for tumorigenic progression of *Rb1*/*Trp53*-mutant
202 preSC (Fig. 1). To validate this finding, we performed a similar experiment using
203 *Rb1*/*Trp53*/*Rbl2*-GEMM in which tumor development is initiated by the loss of *Rbl2*
204 (encoding p130, an RB family member) in addition to *Rb1* and *Trp53* (24). This
205 model represents a subset of human SCLC with loss of all three genes and
206 develops more than a dozen tumors with latency of 6 months as opposed to 1-2
207 tumors with latency of 9-12 months in *Rb1*/*Trp53*-GEMM, thus providing a robust
208 experimental system for measuring the effects of genetic or pharmacological
209 manipulation (25, 26). Intriguingly, *Fgfr1*$^{\Delta/\Delta}$ *Rb1*/*Trp53*/*Rbl2* mice had significantly
210 less tumor burden than *Fgfr1*$^{+/+}$ *Rb1*/*Trp53*/*Rbl2* mice (Fig. 2B). Further, lung
211 tumors in the in the *Fgfr1*$^{\Delta/\Delta}$ *Rb1*/*Trp53*/*Rbl2* mice showed significantly less
212 staining for phosphorylated histone H3 (pHH3), a marker for mitotic cell, than
213 tumors in *Fgfr1*$^{+/+}$ *Rb1*/*Trp53*/*Rbl2* mice (Fig. 2C). These findings suggest that loss
214 of FGFR1 suppresses tumor development through reduced proliferation.
215 To determine whether the decrease in tumor burden is truly due to loss of FGFR1,
216 we validated the recombination of all floxed alleles using genotyping PCR and
217 immunoblot of primary tumor cells from *Fgfr1*$^{\Delta/\Delta}$ *Rb1*/*Trp53*/*Rbl2* mice. Primary
218 cells from one of four randomly selected *Fgfr1*$^{\Delta/\Delta}$ tumors expressed FGFR1 at a
219 level comparable to *Fgfr1*$^{+/+}$ tumor cells (Fig. 3A; Supplementary Fig. S1),
220 indicating incomplete recombination and retention of one *Fgfr1*^{lox} allele.

221 Subsequently, these *Fgfr1*$^{\Delta/lox}$ cells were infected with Ad-Cre in culture,
222 completely lost FGFR1, and gave rise to fewer colonies in soft agar than uninfected
223 *Fgfr1*$^{\Delta/lox}$ cells or Ad-Cre-infected *Fgfr1*$^{+/+}$ cells (Fig. 3A). Immunoblot showed that
224 levels of cleaved Caspase 3 and PARP1 indicative for apoptosis markedly
225 increased in Ad-Cre-infected *Fgfr1*$^{\Delta/lox}$ cells relative to uninfected *Fgfr1*$^{\Delta/lox}$ cells
226 and Ad-Cre-infected *Fgfr1*$^{+/+}$ cells (Fig. 3B). Ad-Cre-infected *Fgfr1*$^{\Delta/lox}$ cells smaller
227 subcutaneous tumors than uninfected *Fgfr1*$^{\Delta/lox}$ cells (Fig. 3C). Similar to the
228 primary tumors with the same genotypes, allograft tumors derived from Ad-Cre-
229 infected *Fgfr1*$^{\Delta/lox}$ cells had significantly less pHH3-positive cells per tumor area
230 than those from uninfected cells (Fig. 3D; Supplementary Fig. S2). These findings
231 suggest that acute deletion of FGFR1 in tumor cells suppressed continued growth
232 of tumor cells through increased cell death and decreased proliferation.
233 Additionally, to determine whether this impact is driven specifically by FGFR1, we
234 used similar methods to examine the impact of deleting *Fgfr2* in the
235 *Rb1*/*Trp53*/*Rbl2*-GEMM. FGFR2 is expressed in the lung epithelium, and the
236 growth and survival of numerous tumor types appear to depend on *FGFR2*
237 amplification or deregulation (27-29). However, loss of *Fgfr2* did not result in
238 decreased tumor burden (Fig. 2C). Taken together, these findings suggest that
239 *Rbl2* loss-driven tumor development depends specifically on FGFR1 signaling.
240

241 ***Loss of p130 induces FGFR1 and the receptor dependency in SCLC***

242 To our knowledge, functional relationships between p130 and FGFR1 have never
243 been documented in cancer. However, p130 was found to repress *Fgfr1*

244 expression during muscle cell differentiation by co-binding with E2F4 at the *Fgfr1*
245 promoter (30). We thus surmised that *Rbl2* loss may amplify FGFR1 dependency
246 in SCLC by increasing FGFR1 expression levels. We first determined whether
247 p130 loss induces FGFR1 expression in preSC. We found that *Rbl2-KO* preSC
248 generated using CRIPSR showed a near-complete loss of p130 but did not induce
249 FGFR1 expression (Fig. 4A). Notably, however, subcutaneous tumors derived
250 from *Rbl2-KO* preSC showed a significant induction of FGFR1 compared to those
251 derived from *Rbl2-WT* preSC (Fig. 4B).
252 To determine whether this inverse correlation between p130 and FGFR1 levels
253 exists across molecular subtypes of SCLC cells, we examined the subcutaneous
254 tumors derived from variants of mutant preSC in which *Crebbp*, *Ep300*, or *Col22a1*
255 was mutated using CRISPR. Loss-of-function mutations in these genes are among
256 the most frequent alterations found in the SCLC genome and have been shown to
257 promote malignant progression of preSC (3, 31). Similar to *Rbl2-KO* tumors,
258 *Crebbp-KO* or *Ep300-KO* tumors expressed FGFR1 but lacked p130, whereas
259 *Col22a1-KO* tumor showed the opposite expression patterns (Fig. 4B).
260 Additionally, a survey of multiple primary tumors developed in *Rb1*/*Trp53*-GEMM
261 and *Rb1*/*Trp53/Rbl2*-GEMM showed a similar inverse correlation between p130
262 and FGFR1 expression (Fig. 4B).
263 We also tested whether p130 regulates FGFR1 expression in malignant SCLC
264 cells. CRISPR-mediated knockout of *Rbl2* increased *Fgfr1* mRNA and FGFR1
265 protein levels in mSCLC (Fig. 4C). Notably, subsequent shRNA-mediated
266 knockdown of *Fgfr1* in *Rbl2*-KO mSCLC cells resulted in these cells giving rise to

267 fewer colonies in soft agar than *Rbl2*-KO cells treated with a scrambled shRNA
268 control, whereas *Fgfr1* knockdown in *Rbl2-WT* cells did not impact colony-forming
269 ability (Fig. 4D). Taken together, these findings suggest that loss of p130 induces
270 FGFR1 expression and results in the dependency of tumor development on
271 FGFR1 signaling.
272
273 ***FGFR1-dependent SCLC cells require activation of PLCG1***
274 To begin to identify intracellular mediators of FGFR1-driven SCLC development,
275 we examined the phosphorylation status of ERK1/2, AKT1, STAT1, and PLCG1,
276 major transducers downstream of FGFR1 during organ development (12).
277 Phosphorylation of AKT1 and PLCG1 increased in *Fgfr1*-preSC relative to control
278 preSC while that of ERK1/2 and STAT did not change, suggesting lack of activation
279 of ERK1/2 and STAT by FGFR1 (Fig. 5A). This finding was intriguing as FGFR1
280 signaling in SCLC has so far been linked to MEK-ERK pathway (32, 33). We
281 performed similar analysis on human SCLC lines with varying levels of FGFR1,
282 including H82, H209, and H524. Lentiviral shRNA-mediated knockdown of FGFR1
283 significantly reduced growth of H82 and H209 cells in soft agar and reduced
284 phosphorylation of PLCG1, but did not impact the growth of H524 colonies and
285 PLCG1 phosphorylation despite comparable levels of knockdown (Fig. 5B, C). In
286 all cell lines, phosphorylation levels of ERK1/2, AKT1, and STAT1 did not change
287 regardless of FGFR1 expression, further demonstrating a specific functional
288 relationship between FGFR1 and PLCG1 in SCLC (Fig. 5C).

289 To determine the significance of PLCG1 activation in SCLC cells, we tested effects
290 of U73122, a chemical inhibitor of PLCG1, and its structural analog U73344 as an
291 innocuous control (34). Compared with control, U73122 reduced viability of H82
292 and H209 cells in a dose-dependent manner (Fig. 5D) and suppressed their ability
293 to give rise to colonies in soft agar (Fig. 5D). However, these effects of U73122
294 were not seen for H524 (Fig. 5D), consistent with the observation that this cell line
295 does not respond to FGFR1 for growth. Importantly, treatment of a pan-FGFR
296 inhibitor PD173074 did not affect viability in the tested SCLC lines (Fig. 5D). Taken
297 together, these data suggest that PLCG1 mediates FGFR1 signaling to promote
298 tumorigenic progression of preSC and continued growth of SCLC cells
299 independently of ERK1/2, AKT1, and STAT1.
300 To further explore the mechanism by which FGFR1 drives tumor growth, we
301 performed RNA sequencing and analyzed a total of 1823 genes that were
302 differentially expressed (DE) in *Fgfr1*-preSC (Fig. 6A; Supplementary Data 1).
303 Gene ontology (GO) analysis of DE genes indicated enrichment of GO terms for
304 cell cycle/mitosis and neuron differentiation and development (Fig. 6B;
305 Supplementary Data 2). The GO terms related to neuron differentiation were
306 further enriched in top 228 DE genes (with 1.5-fold or higher changes in
307 expression) (Fig. 6C; Supplementary Data 3). Enrichment of these GO terms
308 reflected the upregulation of *Rhoa*, *Gli3*, *Etv4*, *Arx*, and *Lif* and downregulation of
309 *Nefl*, *Chl1*, *Dcx* , *Dcc*, *Slitrk3*, *Nr2e1*, and *Bdnf* (Fig. 6A). These results suggest
310 that, in addition to promoting cell cycle, FGFR1 signaling regulates neural
311 differentiation in cells progressing from precancerous neuroendocrine cells to

312 neuroendocrine tumor. This observation is consistent with established roles of
313 FGFR1 in proliferation of neural progenitor cells and neural development (35), and
314 with recent studies showing that dysregulation in neural differentiation is a major
315 event associated with SCLC progression (36, 37).
316

317 **Discussion**

318

319 Here we report for the first time a direct role for nonamplified FGFR1 in SCLC
320 development. *Fgfr1* knockout significantly inhibited tumor growth in various SCLC
321 models, notably in human SCLC lines that have previously shown little sensitivity
322 to existing pharmacological inhibitors (8). While previous studies utilizing FGFR1
323 inhibition in human cell lines have focused on *FGFR1* amplification as a biomarker
324 for drug sensitivity, our findings suggest that FGFR1 expression may confer
325 sensitivity as well, including in subtypes that lack *FGFR1* amplification.

326

327 Little is known about regulators of FGFR1 expression in cancer, and further study
328 of these regulators would provide insight into the heterogeneity in FGFR1
329 dependency among SCLC patient tumors. Our study shows that p130 loss, found
330 in a subset of SCLC patient tumors, induces FGFR1 expression and is sufficient
331 to render p130-deficient mouse tumor dependent on the receptor. The role of p130
332 loss in FGFR1 induction is permissive as it appears to require additional unknown
333 factor present in transforming or malignant cells, which may not be present in
334 preSC. During myogenesis, *Fgfr1* expression is induced in myoblast by complexes
335 containing the Sp1 transcription factor, RB family member p107, and E2F4, and is
336 inhibited in myogenic cells by p130-E2F4 complexes (30). While Sp1, RB family
337 member p107, and E2F4 are variably expressed in SCLC (11, 38, 39), their
338 involvement in the regulation of FGFR1 is not known, and it will be interesting to
339 assess whether these factors also impact FGFR1 dependency.

340

341 Despite the importance of FGFR1 as a prognostic and therapeutic biomarker, the
342 intracellular pathways downstream of FGFR1 have been poorly defined. Our
343 findings indicate that PLCG1 is a critical mediator of FGFR1 signaling in SCLC
344 whereas other pathways, including the ERK pathway, do not appear consistently
345 engaged. PLCG1 is a member of the phospholipase C (PLC) family of enzymes.
346 When activated by growth factor receptors, PLCG1 hydrolyzes
347 phosphatidylinositol 4,5-bisphsphate (PIP_2) to generate inositol 1,4,5-triphosphate
348 (IP_3) and diacylglycerol (DAG). IP_3 then trigger Ca^{2+} release and signaling while
349 DAG activates protein kinase C (PKC), giving rise to various intracellular signaling
350 cascades that control proliferation, differentiation, morphology, and migration in
351 multiple cell types (40). The functional impact of the interaction between FGFR1
352 and PLCG1 has remained poorly understood. Almost two decades ago, the first
353 reports establishing their interaction suggested that it is not critical for mitogenesis
354 (41, 42). More recently, PLCG1 has been shown to mediate FGFR1 signaling in
355 maintaining the differentiation capacity of adult neural stem cells (43). Our data
356 show that PLCG1 activation cooccurs with transcriptomic change related to neural
357 differentiation during FGFR1-driven tumorigenesis, and thus suggest a role for
358 PLCG1 in regulating neuroendocrine differentiation in SCLC. Our findings help add
359 SCLC to the growing list of malignancies in which the activity of PLCG1 is
360 implicated and indicate PLCG1 as a potential therapeutic target in SCLC (44-48).
361

362 Our findings are in line with those of previous studies in which the activation of
363 ERK1/2 and AKT varied among SCLC primary tumors and did not strongly
364 correlate with disease-free or overall survival (49, 50). The role of the ERK pathway
365 in FGFR signaling in SCLC remains unclear. A hyperactive RAF-MEK-ERK
366 pathway has been shown to be tumor-suppressive in SCLC cell lines, in contrast
367 to the oncogenic role of this pathway in non-small cell lung cancer cells (10, 11).
368 Further, in a recent study in *Rb1/Trp53-GEMM*, constitutive FGFR1 activation
369 suppressed the development of SCLC originating from CGRP-positive
370 neuroendocrine cells while promoting the tumor development from keratin 14
371 (K14)-positive airway epithelial cells (13). These studies suggest that whether
372 FGFR1 and the ERK pathway are oncogenic in SCLC may depend on cell of origin.
373 Importantly, our findings demonstrate an oncogenic role for FGFR1 in SCLC
374 tumors with neuroendocrine origin. We surmised that differences in FGFR1
375 dependency may be due to on the extent of signaling from constitutively active
376 versus wild-type of FGFR1 and the interactions between FGFR1 and its signal
377 transducers.
378
379 Taken together, our identification of two novel players in in FGFR1 signaling,
380 PLCG1 and p130, shed light on the mechanism of FGFR1-driven SCLC
381 development and homeostasis, and may facilitate the development of biomarkers
382 for SCLC subtypes appropriate for FGFR1-targeted therapies, as well as targeted
383 therapeutic strategies for SCLC.

Acknowledgements

We thank Drs. Anton Berns, Tyler Jacks, Julien Sage, Juha Partanen, and David Ornitz for sharing *Trp53*^{lox}, *Rb1*^{lox}, *Rbl2*^{lox}, *Fgfr1*^{lox} and *Fgfr2*^{lox} mice, respectively. We thank J. Hsu, J. Sage, and C. Dunn for comments on the manuscript. This work was supported by National Institutes of Health (NCI R01CA194461; U01CA224293; R03CA215777) and American Cancer Society (RSG-15-066-01-TBG) to K-S. P. We also thank S. Vanhoose and her team at the Research Histology Core and the experts of Genome Analysis and Technology Core at the University of Virginia Cancer Center and Biostatistics and Bioinformatics Shared Resources at the H. Lee Moffitt Cancer Center & Research Institute, which are supported by the National Cancer Institute grants (P30CA044579 and P30CA076292).

397 **Figure Legends**

398

399 **Fig. 1. Increased FGFR1 promotes SCLC development**

400 **(A)** RT-qPCR and immunoblot for *Fgfr1* mRNA normalized to *ARBPP0* and
401 FGFR1 protein in preSC and mSCLC (n=3 replicates per cell type). GAPDH blot
402 verifies equal loading of total proteins. (**B)** Left, expression of FGFR1 in preSC
403 infected with empty vector (control preSC) or an FGFR1 expression construct
404 (*Fgfr1*-preSC); ACTB blot verifies equal loading of total proteins. Middle,
405 representative images of soft agar colonies formed by control and *Fgfr1*-preSC.
406 Right, quantification of colonies >0.2mm in diameter (unpaired t-test n=3 replicates
407 per cell type). (**C)** Left, representative image of subcutaneous tumors (arrow) in
408 athymic nude mice (n=5 mice per cell type). Right, quantification of tumor
409 development of subcutaneous tumors >1.5cm in diameter (unpaired t-test n=5
410 mice per cell type); Relative tumor growth represents tumor weight (g) divided by
411 latency (days after allograft). (**D)** Representative image of hematoxylin-eosin
412 (H&E) stained section of *Fgfr1*-preSC-derived subcutaneous tumors and, right, of
413 immunostaining for calcitonin gene-related peptide (CGRP, green). DAPI stains for
414 nuclei (blue). Asterisk indicates non-tumor area. Statistical tests performed using
415 unpaired t-test (ns: not significant). Scale bars: B, 5mm; D, 100μm. Error bars
416 represent standard deviation.

417

418 **Fig. 2. Deletion of *Fgfr1* suppresses SCLC development in vivo**

419 Left, representative images of H&E stained or immunostained sections of the lungs
420 from different SCLC GEMMs and right, quantification of tumor burden (tumor
421 area/lung area) or phosphorylated histone H3 (pHH3)-positive cells per tumor area
422 in **(A)** *Fgfr1*$^{+/+}$ *vs. Fgfr1*$^{\Delta/\Delta}$ *Rb1/Trp53* (n=6 and n=6, respectively), **(B, C)** *Fgfr1*$^{+/+}$
423 *vs. Fgfr1*$^{\Delta/\Delta}$ *Rb1/Trp53/Rbl2* (n=10 and n=10, respectively); in panel **C**, pHH3 stain
424 in green and DAPI in blue. Arrows indicate pHH3-positive nuclei, **(D)** *Fgfr2*$^{+/+}$ *vs.*
425 *Fgfr2*$^{\Delta/\Delta}$ *Rb1/Trp53/Rbl2* n=7 and n=5, respectively). Statistical tests performed
426 using unpaired t-test (ns: not significant). Error bars represent standard deviation.
427 Scale bars: A, B, D, 5mm; C, 50μm.
428
429 **Fig. 3. FGFR1 is critical for continued growth of tumor cells**
430 **(A)** Left, immunoblot for FGFR1 in primary cells derived from the lung tumors in
431 *Fgfr1*$^{+/+}$ and *Fgfr1*$^{lox/lox}$ *Rb1/Trp53/Rbl2*-GEMM infected with Ad-Cre. The cells
432 from one of the *Fgfr1*$^{lox/lox}$ mice show little reduction of FGFR1, indicating
433 incomplete recombination of floxed *Fgfr1* alleles (*Fgfr1*$^{\Delta/lox}$). Following Ad-Cre
434 infection, these cells completely lose FGFR1 expression. Middle, representative
435 images of soft agar colonies formed by *Fgfr1*$^{+/+}$ and *Fgfr1*$^{\Delta/lox}$ *Rb1/Trp53/Rbl2* cells
436 in soft agar 3 weeks following Ad-Cre infection. Right, quantification of colonies
437 >0.2mm in diameter (n=3 replicates per cell type). **(B)** Immunoblot for cleaved and
438 total Caspase 3 and PARP1 in *Fgfr1*$^{+/+}$ and *Fgfr1*$^{\Delta/lox}$ *Rb1/Trp53/Rbl2* cells with or
439 without Ad-Cre infection. Cleaved proteins are a marker for apoptosis and FGFR1
440 blot verifies loss of FGFR1 expression in Ad-Cre infected *Fgfr1*$^{\Delta/lox}$ cells. GADPH
441 blot verifies equal loading of total proteins. **(C)** Top, volumes of tumors (n=6)

442 generated from subcutaneous injection of *Fgfr1*$^{\Delta/lox}$ *Rb1/Trp53/Rbl2* cells with or
443 without Ad-Cre infection. Bottom, quantification of tumor development of
444 subcutaneous tumors >1.5cm in diameter; relative tumor growth represent tumor
445 weight (g) divided by latency (days after allograft). **(D)** Quantification of pHH3
446 staining in allograft tumors derived from *Fgfr1*$^{\Delta/lox}$ *Rb1/Trp53/Rbl2* cells with or
447 without Ad-Cre infection. Statistical tests performed using unpaired t-test. Error
448 bars represent standard deviation.
449
450 **Fig. 4. p130 loss induces FGFR1 expression and dependency**
451 **(A)** Immunoblots for FGFR1 and p130 in control and *Rbl2-KO* preSC (left) and in
452 preSC-derived subcutaneous tumors (right). (**B)** Immunoblots for FGFR1 and p130
453 in the subcutaneous tumors generated from control and various targeted preSC
454 (top) and in primary lung tumors developed in *Rb1/Trp53*-mutant and
455 *Rb1/Trp53/Rbl2*-mutant GEMMs (bottom). Asterisk indicates a non-specific band.
456 (**C**) Left, RT-qPCR for *Fgfr1* mRNA normalized to *ARBPP0*. Right, immunoblots
457 for FGFR1 and p130 in control and *Rbl2-KO* preSC. (**D**) Left, immunoblots for
458 FGFR1 in control and *Rbl2-KO* preSC after shRNA-mediated knockdown of *Fgfr1*.
459 Middle, representative images of soft agar colonies formed by control and *Fgfr1*-
460 knockdown cells. Right, quantification of colonies >0.2mm in diameter (n=3 per cell
461 type). ACTB blot verifies equal loading of total proteins. Statistical tests performed
462 using unpaired t-test (ns: not significant). Error bar represents standard deviation.
463 Scale bar: 5mm.
464

465 **Fig. 5. FGFR1-dependent SCLC cells require activation of PLCG1**

466 **(A)** Immunoblot for phosphorylated forms and respective total protein in control
467 and *Fgfr1*-preSC. ACTB blot verifies equal loading of total proteins. (**B)**
468 Representative images of soft agar colonies formed from human SCLC lines with
469 FGFR1 knockdown (top) and quantification of colonies >0.2mm in diameter
470 (bottom) (n=3 replicates per cell type). (**C)** Immunoblot for phosphorylated and
471 respective total protein in human SCLC lines with FGFR1 knockdown. (**D)** Left,
472 viability of human SCLC lines treated with U73122 (PLCG1 inhibitor) and U73343
473 (innocuous analog of U73122) once for 4 days, as measured by MTT assay.
474 Middle, representative images of soft agar culture of human SCLC lines treated
475 with 1μM U73122 and U73343 every three days for 14 days (H82 and H524) or 21
476 days (H209) and quantification of colonies (>0.2mm) in diameter (n=3 replicates
477 per cell line). Right, viability of human SCLC lines treated with PD173074 (pan-
478 FGFR inhibitor) once for 4 days, as measured by MTT assay. Statistical tests
479 performed using unpaired t-test (ns: not significant). Error bar represents standard
480 deviation. Scale bars: 5mm.

481

482 **Fig. 6. FGFR1 induces transcriptome-wide change in the expression of genes**
483 **involved in proliferation and differentiation**

484 **(A)** Volcano plot showing differential gene expression between control and *Fgfr1*-
485 preSC; changes in gene expression are significant above the red horizontal line,
486 with an FDR-adjusted *p*-value < 0.05, and red and blue dots indicate genes with a
487 an 1.5-fold or higher increase or decrease in expression. FDR: false discovery rate.

488 **(B),** Gene ontology (GO) terms enriched in genes differentially expressed (DE) in
489 *Fgfr1*-preSC relative to control preSC (FDR-adjusted *p*-value < 0.05). Bottom**,**
490 summary of GO terms enriched in top DE genes with an 1.5-fold or higher increase
491 or decrease in expression.

492 **References**
493

494 1. Byers LA, Rudin CM. Small cell lung cancer: where do we go from here?
495 Cancer **2015**;121:664-72

496 2. Peifer M, Fernandez-Cuesta L, Sos ML, George J, Seidel D, Kasper LH*, et*
497 *al.* Integrative genome analyses identify key somatic driver mutations of
498 small-cell lung cancer. Nat Genet **2012**;44:1104-10

499 3. George J, Lim JS, Jang SJ, Cun Y, Ozretic L, Kong G*, et al.* Comprehensive
500 genomic profiles of small cell lung cancer. Nature **2015**;524:47-53

501 4. Voortman J, Lee JH, Killian JK, Suuriniemi M, Wang Y, Lucchi M, *et al.*
502 Array comparative genomic hybridization-based characterization of genetic
503 alterations in pulmonary neuroendocrine tumors. Proc Natl Acad Sci U S A
504 **2010**;107:13040-5

505 5. Zhang L, Yu H, Badzio A, Boyle TA, Schildhaus HU, Lu X, *et al.* Fibroblast
506 Growth Factor Receptor 1 and Related Ligands in Small-Cell Lung Cancer.
507 J Thorac Oncol **2015**; 10:1083-90.

508 6. Desai A, Adjei AA. FGFR Signaling as a Target for Lung Cancer Therapy.
509 J Thorac Oncol **2016**;11:9-20

510 7. Pardo OE, Latigo J, Jeffery RE, Nye E, Poulsom R, Spencer-Dene B*, et al.*
511 The fibroblast growth factor receptor inhibitor PD173074 blocks small cell
512 lung cancer growth in vitro and in vivo. Cancer Res **2009**;69:8645-51

513 8. Sos ML, Dietlein F, Peifer M, Schottle J, Balke-Want H, Muller C*, et al.* A
514 framework for identification of actionable cancer genome dependencies in
515 small cell lung cancer. Proc Natl Acad Sci U S A **2012**;109:17034-9

516 9. Thomas A, Lee JH, Abdullaev Z, Park KS, Pineda M, Saidkhodjaeva L*, et*
517 *al.* Characterization of fibroblast growth factor receptor 1 in small-cell lung
518 cancer. J Thorac Oncol **2014**;9:567-71

519 10. Ravi RK, Weber E, McMahon M, Williams JR, Baylin S, Mal A*, et al.*
520 Activated Raf-1 causes growth arrest in human small cell lung cancer cells.
521 J Clin Invest **1998**;101:153-9

522 11. Ravi RK, Thiagalingam A, Weber E, McMahon M, Nelkin BD, Mabry M. Raf-
523 1 causes growth suppression and alteration of neuroendocrine markers in
524 DMS53 human small-cell lung cancer cells. Am J Respir Cell Mol Biol
525 **1999**;20:543-9

526 12. Ornitz DM, Itoh N. The Fibroblast Growth Factor signaling pathway. Wiley
527 Interdiscip Rev Dev Biol **2015**;4:215-66

13. Ferone G, Song JY, Krijgsman O, van der Vliet J, Cozijnsen M, Semenova EA*, et al.* FGFR1 Oncogenic Activation Reveals an Alternative Cell of Origin of SCLC in Rb1/p53 Mice. Cell Rep **2020**;30:3837-50 e3

14. Meuwissen R, Linn SC, Linnoila RI, Zevenhoven J, Mooi WJ, Berns A. Induction of small cell lung cancer by somatic inactivation of both Trp53 and Rb1 in a conditional mouse model. Cancer Cell **2003**;4:181-9

15. Gazdar AF, Savage TK, Johnson JE, Berns A, Sage J, Linnila RI, *et al.* The comparative pathology of genetically engineed mouse models for neuroendocrine carcinomas of the lung. J Thorac Oncol **2015**;10:553-64

16. Kim DW, Wu N, Kim YC, Cheng PF, Basom R, Kim D*, et al.* Genetic requirement for Mycl and efficacy of RNA Pol I inhibition in mouse models of small cell lung cancer. Genes Dev **2016**;30:1289-99

17. Trokovic R, Trokovic N, Hernesniemi S, Pirvola U, Vogt Weisenhorn DM, Rossant J*, et al.* FGFR1 is independently required in both developing mid- and hindbrain for sustained response to isthmic signals. EMBO J **2003**;22:1811-23

18. Yu K, Xu J, Liu Z, Sosic D, Shao J, Olson EN*, et al.* Conditional inactivation of FGF receptor 2 reveals an essential role for FGF signaling in the regulation of osteoblast function and bone growth. Development **2003**;130:3063-74

19. DuPage M, Dooley AL, Jacks T. Conditional mouse lung cancer models using adenoviral or lentiviral delivery of Cre recombinase. Nat Protoc **2009**;4:1064-72

20. Trapnell C, Pachter L, Salzberg SL. TopHat: discovering splice junctions with RNA-Seq. Bioinformatics **2009**;25:1105-1111.

21. Anders S, Pyl PT, Huber W. HTSeq--a Python framework to work with high-throughput sequencing data. Bioinformatics **2015**;31:166-169.

22. Love MI, Huber W, Anders S. Moderated estimation of fold change and dispersion for RNA-seq data with DESeq2. Genome Biol **2014**;15:550.

23. McFadden DG, Papagiannakopoulos T, Taylor-Weiner A, Stewart C, Carter SL, Cibulskis K*, et al.* Genetic and clonal dissection of murine small cell lung carcinoma progression by genome sequencing. Cell **2014**;156:1298-311

24. Schaffer BE, Park KS, Yiu G, Conklin JF, Lin C, Burkhart DL*, et al.* Loss of p130 accelerates tumor development in a mouse model for human small-cell lung carcinoma. Cancer Res **2010**;70:3877-83

563 25. Park KS, Martelotto LG, Peifer M, Sos ML, Karnezis AN, Mahjoub MR*, et*
564 *al.* A crucial requirement for Hedgehog signaling in small cell lung cancer.
565 Nat Med **2011**;17:1504-8

566 26. Sen T, Tong P, Stewart CA, Cristea S, Valliani A, Shames DS*, et al.* CHK1
567 Inhibition in Small-Cell Lung Cancer Produces Single-Agent Activity in
568 Biomarker-Defined Disease Subsets and Combination Activity with
569 Cisplatin or Olaparib. Cancer Res **2017**;77:3870-84

570 27. Arman E, Haffner-Krausz R, Gorivodsky M, Lonai P. Fgfr2 is required for
571 limb outgrowth and lung-branching morphogenesis. Proc Natl Acad Sci U S
572 A **1999**;96:11895-9
573
574 28. Yuan T, Klinkhammer K, Liu H, Gao S, Yuan J, Hopkins S, *et al.* Temporale
575 Expression of Fgfr1 and 2 During Lung Development, Homeostasis, and
576 Regeneration. Front Pharmacol **2020**;11:120
577
578 29. Pearson A, Smyth E, Babina IS, Herrera-Abreu MT, Tarazona N, Peckitt C*,*
579 *et al.* High-Level Clonal FGFR Amplification and Response to FGFR
580 Inhibition in a Translational Clinical Trial. Cancer Discov **2016**;6:838-51

581 30. Parakati R, DiMario JX. Dynamic transcriptional regulatory complexes,
582 including E2F4, p107, p130, and Sp1, control fibroblast growth factor
583 receptor 1 gene expression during myogenesis. J Biol Chem
584 **2005**;280:21284-94

585 31. Jia D, Augert A, Kim DW, Eastwood E, Wu N, Ibrahim AH, et al. Crebbp
586 Loss Drives Small Cell Lung Cancer and Increases Sensitivity to HDAC
587 Inhibition. Cancer Discovery **2018**;8:1422-1437.

588 32. Pardo OE, Acaro A, Salerno G, Tetley TD, Valovka T, Gout I, *et al*. Novel
589 cross talk between MEK and S6K2 in FGF-2 induced proliferation of SCLC
590 cells. Oncogene 2001; 20:7658-67

591 33. Wang K, Ji W, Yu Y, Li Z, Niu X, Xia W*, et al.* FGFR1-ERK1/2-SOX2 axis
592 promotes cell proliferation, epithelial-mesenchymal transition, and
593 metastasis in FGFR1-amplified lung cancer. Oncogene **2018**;37:5340-54

594 34. Bleasdale JE, Bundy GL, Bunting S, Fitzpatrick FA, Huff RM, Sun FF*, et al.*
595 Inhibition of phospholipase C dependent processes by U-73, 122. Adv
596 Prostaglandin Thromboxane Leukot Res **1989**;19:590-3

597 35. Ohkubo Y, Uchida AO, Shin D, Partanen J, Vaccarino FM. Fibroblast growth
598 factor receptor 1 is required for the proliferation of hippocampal progenitor
599 cells and for hippocampal growth in mouse. J Neurosci **2004**;24:6057-69

600 36. Denny SK, Yang D, Chuang CH, Brady JJ, Lim JS, Gruner BM *et al*. Nfib
601 Promotes Metastasis through a Widespread Increase in Chromatin
602 Accessibility. Cell **2016**;66:328-342.

603 37. Yang D, Qu F, Cai H, Chuang CH, Lim JS, Jahchan N *et al*. Axon-like
604 protrusions promote small cell lung cancer migration and metastasis. Elife
605 **2019**;8.

606 38. Kim WY, Jang JY, Jeon YK, Chung DH, Kim YG, Kim CW. Syntenin
607 increases the invasiveness of small cell lung cancer cells by activating p38,
608 AKT, focal adhesion kinase and SP1. Exp Mol Med 2014;46:e90.
609
610 39. Brown KC, Witte TR, Hardman WE, Luo H, Chen YC, Carpenter AB, et al.
611 Capsaicin displays anti-proliferative activity against human small cell lung
612 cancer in cell culture and nude mice models via E2F pathway. PLoS One
613 2010;5:e10243.

614 40. Koss H, Bunney TD, Behjati S, Katan M. Dysfunction of phospholipase Cg
615 in immune disorders and cancer. Trends Biochem Sci 2014;39:603-11.

616 41. Peters KG, Marie J, Wilson E, Ives HE, Esobedo J, Del Rosario M, *et al.*
617 Point mutation of an FGF recentor abolishes phosphatidylinositol turnover
618 and Ca^{2+} flux but nor mitogenesis. Nature 1992;358:678-681

619 42. Mohammadi M, Dionne CA, Li W, LiN, Spival T, Honegger M, et al. Point
620 mutation in FGF receptor eliminates phosphatidylinositol hydrolysis without
621 affecting mitogenesis. Nature 1992;358:681-684.

622 43. Vaque JP, Gomex-Lopez G, Monsalvez V, Valera I, Martinez N, Perez C,
623 *et al.* PLCG1 mutations in cutaneous T-cell lymphomas. Blood
624 **2014**;123:2034-43.

625 44. Kunze K, Spieker T, Gamerdinger U, Nau K, Berger J, Dreyer T, *et al.*
626 Arecurrent activating PLCG1 mutation in cardiac angiosarcomas increases
627 apoptosis resistance and invasiveness of endothelial cells. Cancer Res
628 **2014**;74:6173-83.

629 45. Gouaze-Andersson V, Delmas C, Taurance M, Martinex-Gala J, Evrard S,
630 Mazoyer S, *et al.* FGFR1 Induces Glioblastoma Resistance through the
631 PLCγ1/Hif1α Pathway. Cancer Res **2016**;76:3036-44.

632 46. Walker K, Boyd NH, Anderson JC, Willey CD, Hjelmeland AB. Kinome
633 profiling of glioblastoma cells revelas PLCG1 as a target in restricted
634 glucose. Biomarker Res **2018**;6:22.

635 47. Tang W, Zhou Y, Sun D, Dong L, Xia J, Yang B. Oncogenic role of
636 phospholipase C-γ1 in progression of hepatocellular carcinoma. Hepatol
637 Res **2019**;49:559-569.

638 48. Ma DK, Ponnusamy K, Song MR, Ming GI, Song H. Molecualr genetic
639 analysis of FGFR1 signalling reveals distinct roles of MAPK and
640 PLAgamma1 activation for self-renewal of adult neural stem cells. Mol Brain
641 2009;2:16.

642 49. Blackhall FH, PintillieM, MIchael M, Leighl N, Feld R, Tsao MS, *et al*.
643 Expression and prognostic significance of kit, protein kinase B, and
644 mitogen-activated protein kinase in patients with small cell lung cancer. Clin
645 Cancer Res **2003**;9:2241-7.

646 50. Schmid K, Bago-Horvath Z, Berger W, Haitel A, Cejka D, Werzowa J, et al.
647 Dual inhibition of EGFR and mTOR pathways in small cell lung cancer. Br
648 J Cancer **2010**;103:622-8.

Fig. 1

A

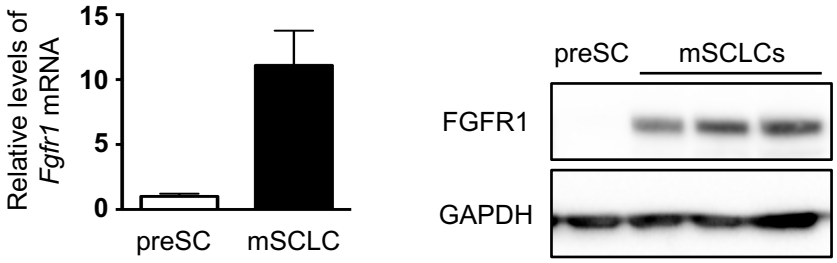
Relative levels of *Fgfr1* mRNA
15
10
5
0
preSC
mSCLC
preSC
mSCLCs
FGFR1
GAPDH

B

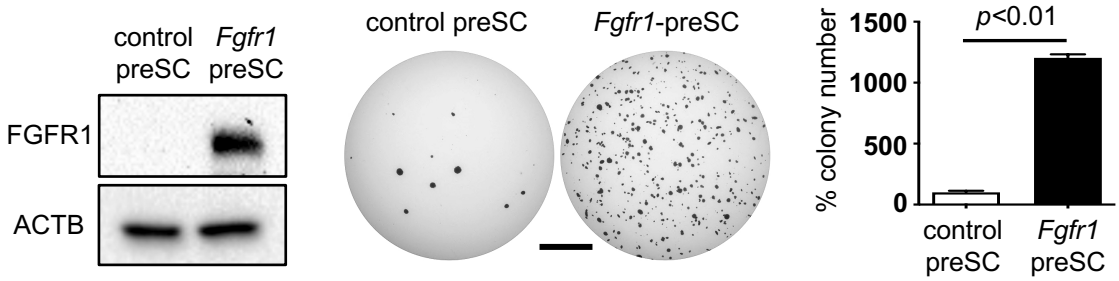
control preSC
Fgfr1 preSC
FGFR1
ACTB
control preSC
Fgfr1-preSC
% colony number
1500
1000
500
0
p<0.01
control preSC
Fgfr1 preSC

C

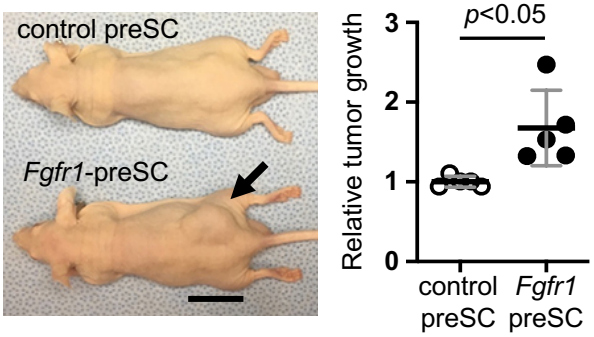
control preSC
Fgfr1-preSC
Relative tumor growth
3
2
1
0
p<0.05
control preSC
Fgfr1 preSC

D

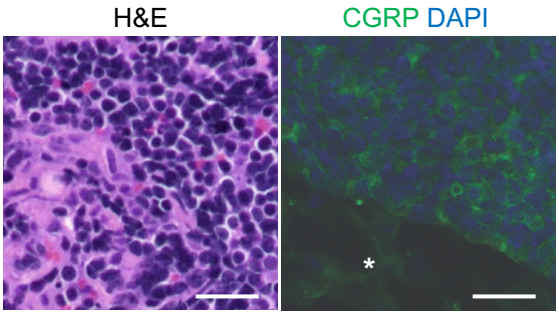
H&E
CGRP DAPI
*

Fig. 2

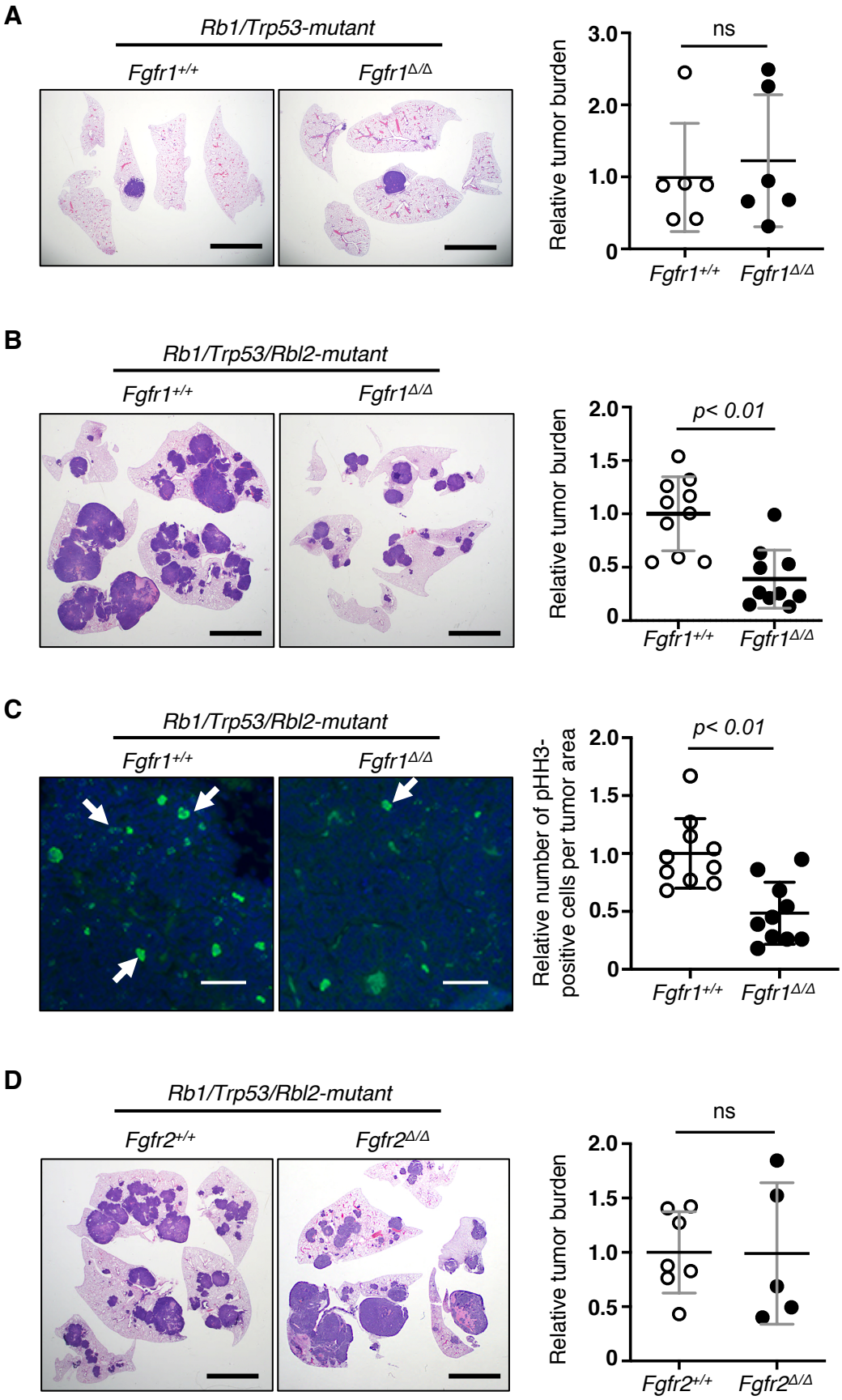
A
Rb1/Trp53-mutant
Fgfr1+/+
Fgfr1Δ/Δ
ns
Relative tumor burden
3.0
2.0
1.0
0
Fgfr1+/+
Fgfr1Δ/Δ
B
Rb1/Trp53/Rbl2-mutant
Fgfr1+/+
Fgfr1Δ/Δ
p< 0.01
Relative tumor burden
2.0
1.5
1.0
0.5
0
Fgfr1+/+
Fgfr1Δ/Δ
C
Rb1/Trp53/Rbl2-mutant
Fgfr1+/+
Fgfr1Δ/Δ
p< 0.01
Relative number of pHH3-positive cells per tumor area
2.0
1.5
1.0
0.5
0
Fgfr1+/+
Fgfr1Δ/Δ
D
Rb1/Trp53/Rbl2-mutant
Fgfr2+/+
Fgfr2Δ/Δ
ns
Relative tumor burden
2.0
1.5
1.0
0.5
0
Fgfr2+/+
Fgfr2Δ/Δ

Fig. 3

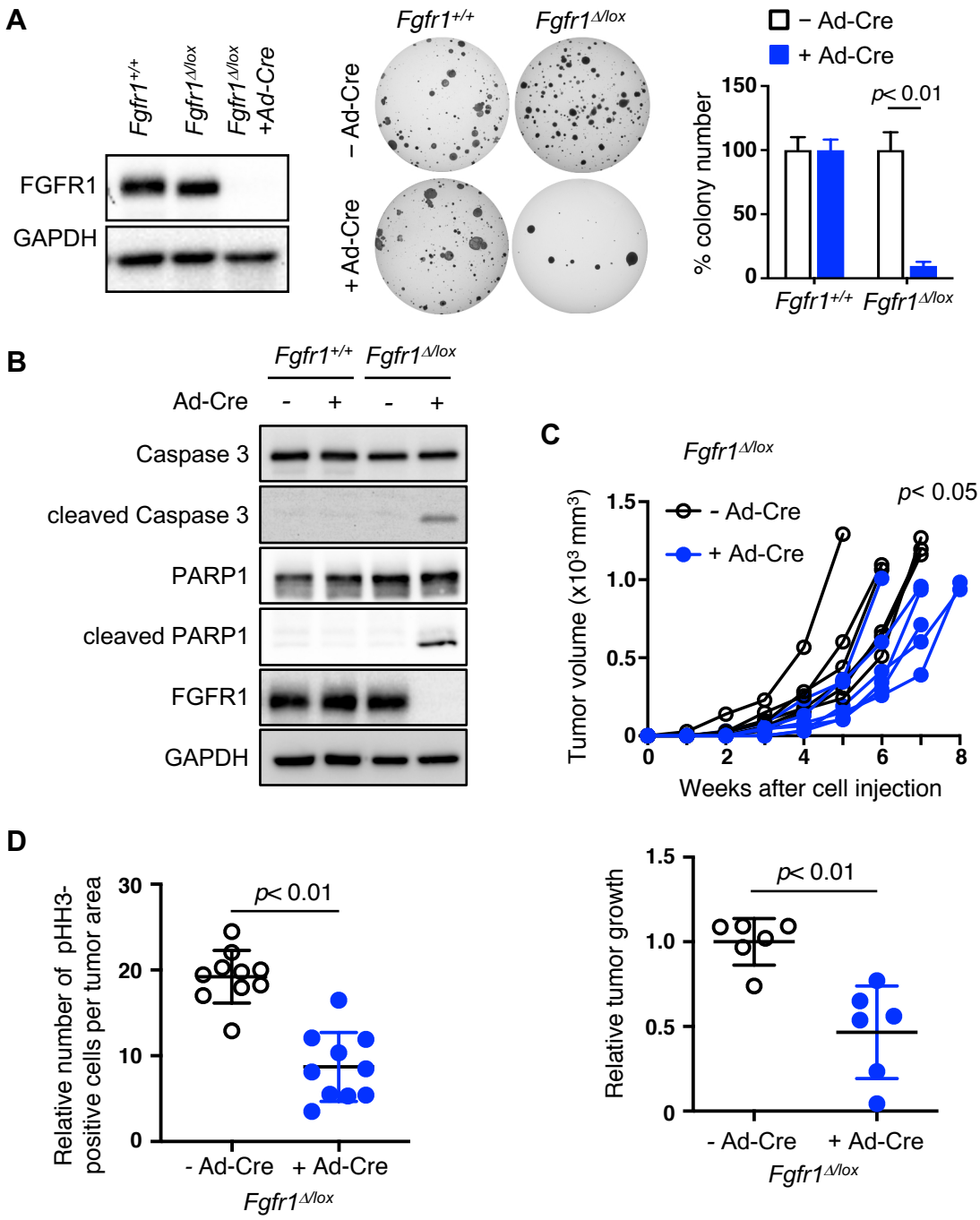
A
Fgfr1+/+
Fgfr1Δ/lox
Fgfr1Δ/lox +Ad-Cre
FGFR1
GAPDH
– Ad-Cre
+ Ad-Cre
Fgfr1+/+
Fgfr1Δ/lox
– Ad-Cre
+ Ad-Cre
% colony number
150
100
50
0
p< 0.01
Fgfr1+/+
Fgfr1Δ/lox
B
Fgfr1+/+
Fgfr1Δ/lox
Ad-Cre - + - +
Caspase 3
cleaved Caspase 3
PARP1
cleaved PARP1
FGFR1
GAPDH
C
Fgfr1Δ/lox
- Ad-Cre
+ Ad-Cre
p< 0.05
Tumor volume (x10³ mm³)
1.5
1.0
0.5
0
0
2
4
6
8
Weeks after cell injection
D
Relative number of pHH3-positive cells per tumor area
30
20
10
0
p< 0.01
- Ad-Cre
+ Ad-Cre
Fgfr1Δ/lox
Relative tumor growth
1.5
1.0
0.5
0
p< 0.01
- Ad-Cre
+ Ad-Cre
Fgfr1Δ/lox

Fig. 4

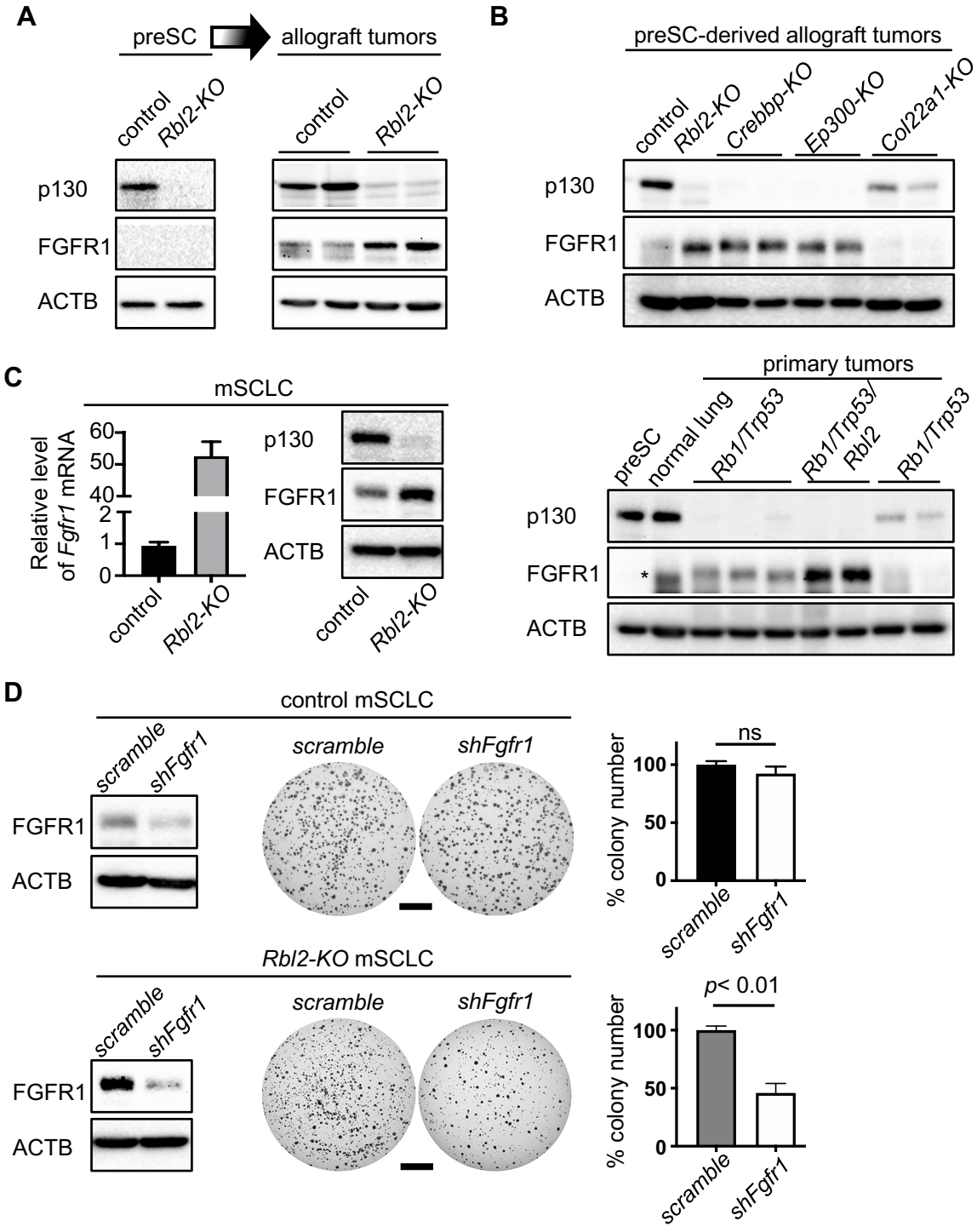
A
preSC
allograft tumors
control
Rbl2-KO
control
Rbl2-KO
p130
FGFR1
ACTB
B
preSC-derived allograft tumors
control
Rbl2-KO
Crebbp-KO
Ep300-KO
Col22a1-KO
p130
FGFR1
ACTB
C
mSCLC
Relative level of Fgfr1 mRNA
60
50
40
2
1
0
control
Rbl2-KO
p130
FGFR1
ACTB
control
Rbl2-KO
primary tumors
preSC
normal lung
Rb1/Trp53
Rb1/Trp53/ Rbl2
Rb1/Trp53
p130
FGFR1
*
ACTB
D
control mSCLC
scramble
shFgfr1
FGFR1
ACTB
scramble
shFgfr1
ns
% colony number
100
50
0
scramble
shFgfr1
Rbl2-KO mSCLC
scramble
shFgfr1
FGFR1
ACTB
scramble
shFgfr1
p< 0.01
% colony number
100
50
0
scramble
shFgfr1

Fig. 5

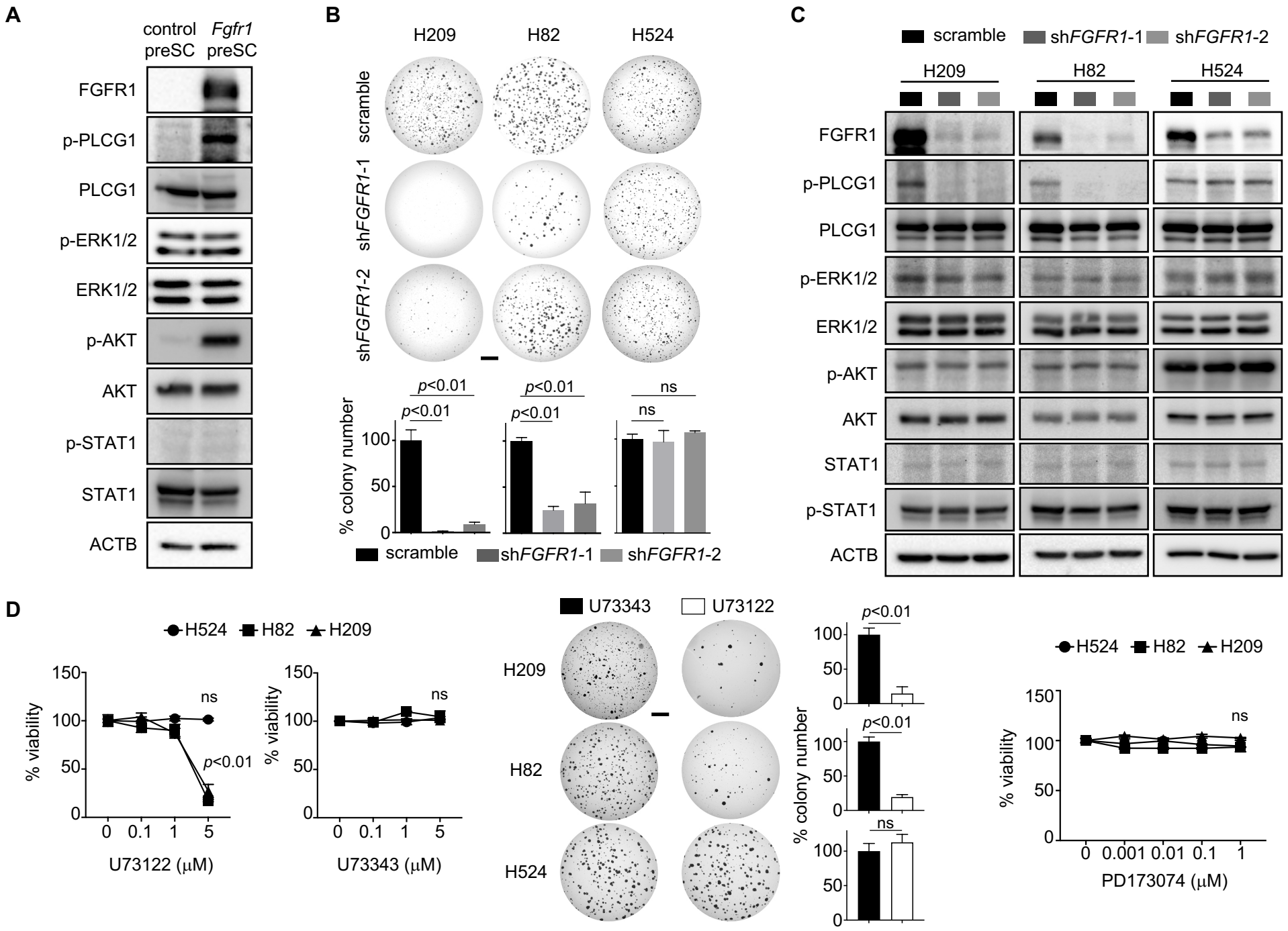
A
control preSC
Fgfr1 preSC
FGFR1
p-PLCG1
PLCG1
p-ERK1/2
ERK1/2
p-AKT
AKT
p-STAT1
STAT1
ACTB
B
H209
H82
H524
scramble
shFGFR1-1
shFGFR1-2
p<0.01
p<0.01
ns
% colony number
100
50
0
scramble
shFGFR1-1
shFGFR1-2
C
scramble
shFGFR1-1
shFGFR1-2
H209
H82
H524
FGFR1
p-PLCG1
PLCG1
p-ERK1/2
ERK1/2
p-AKT
AKT
STAT1
p-STAT1
ACTB
D
H524
H82
H209
% viability
150
100
50
0
ns
p<0.01
0
0.1
1
5
U73122 (μM)
U73343 (μM)
U73343
U73122
H209
H82
H524
% colony number
p<0.01
p<0.01
ns
0
0.001
0.01
0.1
1
PD173074 (μM)

Fig. 6

A

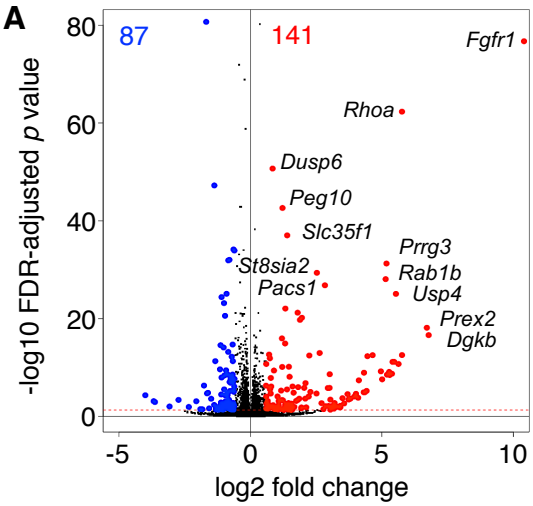

B

GO terms enriched in total DEs	# terms
Neural differentiation, morphogenesis, axonogenesis	15
Cell morphogenesis, differentiation, development	9
Cell cycle, cell division, proliferation	6
Kinase activity, phosphorylation, regulation of kinase	6
Adhesion	2
Cell motion, migration	2
Translation	1
Regulation of transferase activity	1
Regulation of cellular compartment size	1

GO terms enriched in top DEs	# terms
Neural differentiation, morphogenesis, axonogenesis	6
Cell morphogenesis, differentiation, development	4